⌘ *Author's Choice*

THE JOURNAL OF BIOLOGICAL CHEMISTRY VOL. 287, NO. 42, pp. 35565–35575, October 12, 2012

Kcnh1 Voltage-gated Potassium Channels Are Essential for Early Zebrafish Development*[S]

Received for publication, March 19, 2012, and in revised form, August 3, 2012 Published, JBC Papers in Press, August 27, 2012, DOI 10.1074/jbc.M112.363978

Rayk Stengel[‡1], Eric Rivera-Milla[§1], Nirakar Sahoo[‡], Christina Ebert[§], Frank Bollig[§], Stefan H. Heinemann[‡], Roland Schönherr[‡2], and Christoph Englert[§]

From the [‡]Friedrich Schiller University of Jena and Jena University Hospital, Center for Molecular Biomedicine, Department of Biophysics and [§]Leibniz Institute for Age Research-Fritz Lipmann Institute, D-07745 Jena, Germany

Background: Kcnh1 is a voltage-gated potassium channel that is primarily expressed in brain.
Results: Knockdown of kcnh1 in zebrafish delays neural development and causes embryonic lethality.
Conclusion: Kcnh1 is involved in cell proliferation during early zebrafish development.
Significance: The finding that Kcnh1 has basic functions beyond neural signaling will help to elucidate its roles in physiology and cancer formation.

The *Kcnh1* gene encodes a voltage-gated potassium channel highly expressed in neurons and involved in tumor cell proliferation, yet its physiological roles remain unclear. We have used the zebrafish as a model to analyze *Kcnh1* function *in vitro* and *in vivo*. We found that the *kcnh1* gene is duplicated in teleost fish (*i.e. kcnh1a* and *kcnh1b*) and that both genes are maternally expressed during early development. In adult zebrafish, *kcnh1a* and *kcnh1b* have distinct expression patterns but share expression in brain and testis. Heterologous expression of both genes in *Xenopus* oocytes revealed a strong conservation of characteristic functional properties between human and fish channels, including a unique sensitivity to intracellular Ca^{2+}/calmodulin and modulation of voltage-dependent gating by extracellular Mg^{2+}. Using a morpholino antisense approach, we demonstrate a strong *kcnh1* loss-of-function phenotype in developing zebrafish, characterized by growth retardation, delayed hindbrain formation, and embryonic lethality. This late phenotype was preceded by transcriptional up-regulation of known cell-cycle inhibitors (*p21*, *p27*, *cdh2*) and down-regulation of pro-proliferative factors, including *cyclin D1*, at 70% epiboly. These results reveal an unanticipated basic activity of *kcnh1* that is crucial for early embryonic development and patterning.

Kcnh1 is a voltage-gated potassium channel with canonical tetrameric structure and six-transmembrane domain topology. The *Kcnh1* gene was originally named *ether à go-go* (*eag*) as its mutation in *Drosophila melanogaster* induced a rhythmic leg-shaking phenotype under ether anesthesia (1); it is also referred to as *eag1* or $K_v10.1$. *Kcnh1* mutant flies exhibit a high frequency of spontaneous action potentials and enhanced transmitter release in motor neurons (2). In mammals *Kcnh1* expression is almost completely restricted to the brain (3–5), but no specific neuronal function could yet be described. The only physiological function ascribed to vertebrate Kcnh1 channels thus far is a promoting role at the onset of myoblast fusion (6, 7).

An important pathophysiological role for Kcnh1 in cancer formation has been proposed (8) because the human *KCNH1* gene is overexpressed in a broad spectrum of cancers and channel inhibition can reduce cell proliferation (8–11). However, neither the gene expression profile nor the deduced functional properties of Kcnh1 channels provided insight into mechanisms underlying the channel oncogenic potential. Many oncogenes are involved in development, and cancer formation often recapitulates key processes of embryogenesis (12). Thus, it would be instructive to study Kcnh1 during embryonic development, but thus far no suitable vertebrate models have been established.

Recently it became evident that *Danio rerio* (zebrafish) is a valuable model for investigating Kcnh2 (Erg1, $K_v11.1$) channel diseases of the heart (13–18). With respect to physiological functions, Kcnh2 is the best-characterized member of the Kcnh channel family. It is involved in the control of cardiac action potentials, and mutations in *KCNH2* can cause life-threatening cardiac arrhythmias in humans (19–21). *Kcnh2* knockdown in zebrafish was found to mimic the known cardiac phenotype without systemic disturbance of embryo development (13–18).

We evaluated zebrafish as a model organism to study physiological functions of Kcnh1 potassium channels in vertebrates and their potential role in embryogenesis. We identified and cloned two fish orthologs of *KCNH1*, both sharing typical functional properties with human KCNH1 channels. The *kcnh1* genes in zebrafish showed maternal expression, and morpholino-mediated knockdown caused severe and specific developmental anomalies. Our results provide evidence for a novel role of Kcnh1 voltage-gated potassium channels during embryo development and establish the zebrafish as a valuable model to study such functions.

EXPERIMENTAL PROCEDURES

Maintenance of Fish—Zebrafish embryos were obtained from matings of wild-type fish of the TüAB strain that had been

* This work was supported in part by a grant from the Deutsche Forschungsgemeinschaft (SFB 604) (to C. E. and to S. H. H.).
[S] This article contains supplemental Table S1 and Figs. S1–3.
⌘ *Author's Choice*—Final version full access.
[1] Both authors contributed equally to this work.
[2] To whom correspondence should be addressed: Jena University Hospital, Center for Molecular Biomedicine, Dept. of Biophysics, Hans-Knöll-Str. 2, D-07745 Jena, Germany. Tel.: 49-3641-9395680; Fax: 49-3641-9395652; E-mail: Roland.Schoenherr@uni-jena.de.

kept in laboratory stocks in Jena for many generations, according to the local animal care program. Embryos were raised at 28 °C and staged according to Kimmel *et al.* (22).

Bioinformatics—The *kcnh1* genes in zebrafish genome databases were identified using the GenBank™ (www.ncbi.nlm.nih.gov), JGI, Ensembl, and UCSC Genome browsers. Protein and nucleotide databases were searched using BLAT and BLAST algorithms (blastn and tblastn; E-values = e^{-30} as a threshold) using as a reference the human KCNH1 sequence NM_002238 (GenBank™). For phylogenetic and synteny analyses, DNA sequences were edited and analyzed using the DNASTAR package (Lasergene 5.02). Amino acid sequences were aligned using ClustalW and the core matrix PAM-45. Phylogenetic analyses were performed using distance-based methods as neighbor-joining and minimum-evolution incorporated in the MEGA software (23). Reliability of tree topologies was assessed using bootstrapping after 1000 iterations.

Cloning of kcnh1a and kcnh1b Coding Sequences—Total RNA isolated from 24 h post-fertilization (hpf)[3] embryos was treated with DNase I and used as a template for cDNA synthesis using the SuperScript III RT kit (Invitrogen). Gene-specific PCR reactions were set up for three overlapping fragments of each zebrafish *kcnh1* gene (primer information upon request). Resulting overlapping amplicons were used in second and third PCR reactions as templates with the respective primers of the distal ends. Finally, full-length cDNAs were ligated into the pGEM-T vector (Promega) and fully sequenced. Selected clones were digested with BamHI/XbaI and ligated into pGEM-HE (24).

Dominant negative mutants of zebrafish channels (Kcnh1a G438C; Kcnh1b G438C) were constructed using site-directed mutagenesis (QuikChange kit, Stratagene). PCR reactions were performed using the pGEM-HE clones of the corresponding genes as a template and primers carrying the desired mutation. Clones were fully sequenced to confirm the correct mutation. The dominant negative mutant of the human channel (KCNH1 G440C) was as described previously (25).

Whole-mount in Situ Hybridization—Gene-specific probes were amplified by PCR using 24-hpf zebrafish cDNA as the template and the following primers: kcnh1a probe forward (5′-CTG GAA AGA AGT AAC ACT AGC TCA GG-3′), kcnh1a probe reverse (5′-GTG TGT TCG GGA ATG GTT GG-3′), *kcnh1b* probe forward (5′-GGA CAC TTC TCA CGC AAT CTG G-3′), *kcnh1b* probe reverse (5′-GAT ATC CCC CTG CAG ATC TTG C-3′). Amplicons (819 bp for *kcnh1a* and 738 bp for *kcnh1b*) were ligated into pGEM-T vector (Promega) and sequenced. Digoxigenin-labeled antisense riboprobes were generated from linearized vectors (SacII) using the SP6 RNA polymerase (sense riboprobes: NotI and T7 RNA polymerase). Whole-mount *in situ* hybridization was performed essentially as described (26). Probes were detected using anti-digoxigenin alkaline phosphatase and nitro blue tetrazolium/5-bromo-4-chloro-3-indolyl phosphate (Roche Applied Science). For characterization of *kcnh1* morphants, the following markers were used: *ntl* (27), *myoD* (28), *krox20* (29), *atp1a3b* (30), and foxd3, wnt11, and fgf8 (31). Photographs were taken using a Zeiss Axio Imager microscope (Carl Zeiss, Oberkochen, Germany) after embedding stained embryos in 1% methylcellulose or glycerol.

Morpholino Treatment of Zebrafish Embryos—The sequences of the used morpholinos (MOs) are: *kcnh1a* ATG (5′-CAC GGC GGG TCA TGC GCT CCA CTG A-3′), *kcnh1b* ATG (5′-GCG CTG AAG AGC CTC CTG CTA CA-3′), *kcnh1* pan-ATG (5′-CTA GTC CTC TGC GTC CCC CGG CCA T-3′), *kcnh1a* e1i1 (5′-AGG TGC GTC TTA CCG TTA GAC CGT-3′), *kcnh1a* e2i2 (5′-GCA CAA TAT ATC TGT TAC CTG CAA G-3′), *kcnh1b* e1i1 (5′-AGT GTA CAA GGC TTT TCT CAC CGT T-3′), *kcnh1b* e2i2 (5′-ACA GAA ACA TGA AAT CAC CTG CAT G-3′). One to two-cell stage embryos were injected (~5 nl) with different MO concentrations (ranging from 0.1 to 1 mM) and raised at 28.5 °C. As controls, we used a MO (5′-GCG CCA TTG CTT TGC AAG AAT TG-3′) to knock down the Δ113 transcript of *p53* (not expressed before 48 hpf) (32) and a published *kcnh2* ATG-MO (5′-GCG GCG CAC GGG CAT TTT TCA CGC G-3′) (14). Images were generated using the AxioVision software (Zeiss). To test the specificity of ATG-MO, we generated modified pCS2+GFP and pCS2+RFP mRNAs (kindly provided by J. Wittbrodt, Heidelberg) that contained the MO target sequences of *kcnh1a* and *kcnh1b* MO directly upstream of the corresponding start codon (Fig. 6, *A* and *B*). We performed serial injections into 1–2-cell-stage embryos, injecting MO first (0.5 mM final concentration) and then a mix of modified mRNAs (10 ng final concentration each) as described in Table 1. Live embryos (24 hpf) were scored for GFP and RFP signal using epifluorescence Stereo Discovery V8 microscope (Zeiss).

RT-PCR Analysis—Total RNA was isolated from zebrafish embryos, morphants, or zebrafish organs using the RNeasy Mini kit (Qiagen) and treated with DNase. cDNA synthesis was performed using SuperScript III and oligo(dT) primers (Invitrogen). PCR analysis of cDNA was carried out with the Expand High Fidelity PCR system (Roche Applied Science) using gene-specific primers as follows: *kcnh1a* forward (5′-TTT TCT GGA AAA TAT TGT CCG ACG G-3′), *kcnh1a* reverse (5′-GTG GGC TGC AGT TGC TGA AGG-3′), *kcnh1b* forward (5′-GAG AAT ATA GTG CGG CGC TCC-3′), *kcnh1b* reverse (5′-TTT AAG CAC GTT TTC TCC CCG-3′), *kcnh2* forward (5′-ATG CCC GTG CGC CGC G-3′), *kcnh2* reverse (5′-CGA TGT CGT GCA GCG AGG ATG C-3′). Annealing temperatures were: *kcnh1a* primer pair, 60 °C; *kcnh1b* primer pair, 58 °C; *kcnh2* primer pair, 62 °C. For loading control the expression of *bactin* was tested using forward primer (5′-GAG AAG ATC TGG CAT CAC ACC-3′) and reverse primer (5′-AGC TTC TCC TTG ATG TCA CG-3′) at an annealing temperature of 60 °C. For quantitative RT-PCR, total RNA was isolated from 40–50 zebrafish embryos at 70% epiboly stage. 800 ng of RNA was used to synthesize cDNA. PCR analysis was carried out using the SYBR GreenER quantitative PCR super mix for iCycler (Invitrogen) in an iCycler device (96-well format; Bio-Rad). All samples were measured as triplicates and normalized to the corresponding amounts of the housekeeping gene *ef1a* (33), which was measured within the same plate. Relative expression levels where calculated using the $2^{-\Delta\Delta CT}$ method (34) and are based

[3] The abbreviations used are: hpf, hours post fertilization; MO, morpholino; HEDTA, *N*-(2-hydroxyethyl)ethylenediaminetriacetic acid; CaM, calmodulin; RFP, red fluorescent protein.

on two independent experiments. The gene-specific primer set is listed in supplemental Table 1.

Electrophysiological Measurements—Capped mRNA was synthesized *in vitro* using the mMessage mMachine kit (Ambion) and NheI-linearized pGEM-HE constructs containing the respective channel-coding sequence as template. Stage-V *Xenopus laevis* oocytes were surgically obtained under ice water/tricaine anesthesia according to the local animal care program. Manually defolliculated oocytes were microinjected with channel-coding mRNA (<50 nl). For patch clamp measurements the vitelline membrane was removed by enzymatic treatment as described (35). Currents were measured 1–4 days after mRNA injection.

Inside-out Patch Clamp Measurements—Aluminum silicate glass pipettes with resistances of 1–2 megaohms were used for electrodes. An EPC-9 amplifier operated with PatchMaster software (both HEKA Elektronik, Lambrecht, Germany) was used as the patch clamp amplifier. For the I-V measurements in symmetrical K^+, the bath solution contained: 100 mM potassium aspartate, 10 mM EGTA, 15 mM KCl, 10 mM HEPES (pH 8.0 with KOH). The pipette solution was composed of 103.6 mM potassium aspartate, 11.4 mM KCl, 1.8 mM $CaCl_2$, 10 mM HEPES (pH 7.2 with KOH). For the measurement of Ca^{2+}/CaM effects, the solutions used were "1 μM Ca^{2+}" (115 mM potassium aspartate, 10 mM HEDTA, 5 mM $CaCl_2$, 10 mM HEPES (pH 8.0 with KOH)) or "Ca^{2+}-free" (100 mM potassium aspartate, 10 mM EGTA, 15 mM KCl, 10 mM HEPES (pH 8.0 with KOH)). The change of solutions was performed using a multichannel perfusion system, and the pipette tip was placed directly in the middle of streaming solution. His_6-tagged human CaM was prepared as previously described (36).

Non-stationary Noise Analysis from On-cell Membrane Patches—Non-stationary noise analysis was performed from sets of at least 200 successive current sweeps containing responses to depolarizations to −20, 0, 20, 40, and 80 mV. Ensemble variances were compiled from differences of neighboring records (37), and variance-current plots of the activating current phases were simultaneously fitted for all voltages (V) as described (38) to yield the single-channel current $i(V)$, the maximal open probability $P_o(V)$, and the number of active channels.

Two-electrode Voltage Clamp—Currents were recorded at 24.5 ± 0.5 °C using a Turbo-TEC 10CD amplifier (NPI electronic, Tamm, Germany) operated with PatchMaster software (HEKA Elektronik). Filament glass pipettes (Hilgenberg, Malsfeld, Germany) filled with 2 M KCl and having resistances between 0.6 and 0.8 megaohms were used for electrodes. The bath solution (normal frog Ringer) contained 115 mM NaCl, 2.5 mM KCl, 1.8 mM $CaCl_2$, 10 mM HEPES (pH 7.2, NaOH). The addition of 5 mM $MgCl_2$ to this solution is indicated in the figures of the respective experiments. Co-expression of wild-type and dominant negative mutant channels was obtained by microinjection of a 1:1 mix of the corresponding mRNAs. For these experiments 3 independent injections of each RNA mix were performed with 5–10 oocytes per injection.

Data analysis was performed with FitMaster software (HEKA Elektronik) and IgorPro software (WaveMetrics, Lake Oswego, OR). Pooled data are represented as the means ± S.E. (n = number of independent experiments). p values from unpaired Student's t tests are indicated as * (<0.05), ** (<0.01), and *** (<0.001).

RESULTS

Two kcnh1 Genes in Zebrafish—An *in silico* search for putative *KCNH1* (*EAG1*) orthologs in the zebrafish genome yielded four putative candidates. Two of those, located on chromosomes 17 and 22, encode proteins with more than 90% amino acid identity to human KCNH1. The gene on chromosome 17 had already been predicted as *kcnh1* in the Ensembl database (39). The second two hits scored at 86–88% amino acid identity to KCNH1 and represent the orthologs of the closest gene family member *KCNH5* (*EAG2*), located on chromosomes 20 and 13. A phylogenetic analysis comparing human, mouse, and chicken *Kcnh1* and *Kcnh5* genes to the corresponding genes in the fish genomes from medaka, puffer fish, and zebrafish supported this assignment (Fig. 1*A*). These findings are in accordance with the suggested whole-genome duplication that occurred in a common ancestor of teleost fish (40–42). We named the *kcnh1* genes in zebrafish *kcnh1a* (chromosome 17, GenBank™ accession number HQ703597) and *kcnh1b* (chromosome 22, accession number HQ703598). Synteny analysis of the chromosome regions encoding *Kcnh1* loci in human and zebrafish genomes revealed similarities in gene organization for human *KCNH1* and zebrafish *kcnh1a*, whereas the *kcnh1b* locus on zebrafish chromosome 22 showed no obvious overlaps in gene organization (Fig. 1*B*).

Cloning of the zebrafish *KCNH1* orthologs, both being assembled from 11 exons, revealed that all exon borders are conserved between fish and human (Fig. 1*C*). The only two exons with differences in length are exons 1 and 11. Conservation at the level of amino acids is lowest (34% identity) in the second half of the cytosolic carboxyl termini of the predicted channel proteins (Fig. 1*C*). By contrast, all six membrane-spanning segments, the amino-terminal Per-ARNT-Sim domain and the carboxyl-terminal cyclic nucleotide binding domain as well as three CaM binding motifs are highly conserved between human and zebrafish channel proteins (Fig. 1, *C* and *D*).

Kcnh1a and kcnh1b Code for Functional Voltage-gated Potassium Channels with Typical KCNH1-like Characteristics—We expressed both zebrafish *kcnh1* genes in *X. laevis* oocytes by injection of *in vitro* transcribed mRNA. Electrophysiological recordings revealed the formation of potassium channels with functional properties similar to human KCNH1 (Fig. 2). In inside-out patch clamp experiments, stepwise depolarization of the membrane potential elicited K^+ currents very similar in amplitude as well as in activation and deactivation kinetics (Fig. 2*A*). Overall, the steady-state current-voltage dependences of the three channels largely superimposed in the voltage range explored (Fig. 2*B*). The currents measured at the ends of depolarizing pulses and peak tail currents were plotted *versus* depolarization voltages and analyzed by fits with 4th-order Boltzmann functions. The half-maximal gate activation voltages were similar (KCNH1, −65.1 ± 2.3 mV; Kcnh1a, −54.0 ± 2.4 mV; Kcnh1b, −55.3 ± 4.5 mV), whereas the corresponding slope factor was lower for Kcnh1b (17.2 ± 0.5 mV) in comparison to KCNH1 (24.7 ± 1.3 mV) and Kcnh1a (21.0 ± 0.6 mV) (Fig. 2*C*). Single-channel characteristics were estimated by

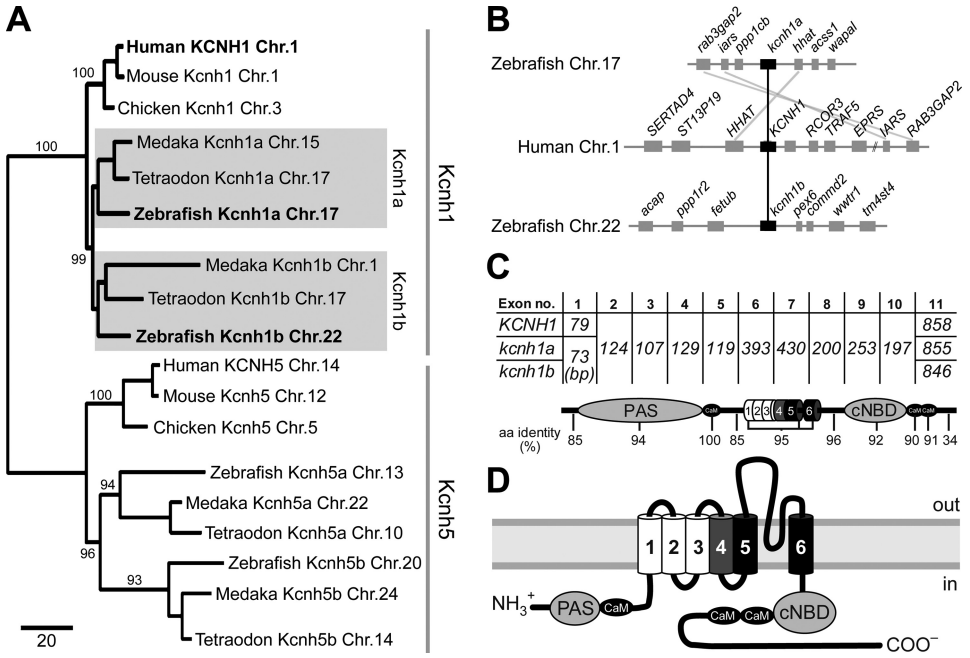

FIGURE 1. **Conserved Kcnh1 channels in zebrafish and man.** *A*, shown is a distance-based phylogenetic tree of *kcnh1* and *kcnh5* genes in three fish genomes and their human, mouse, and chicken orthologs. Fish *kcnh1a* and *kcnh1b* paralogs are *highlighted with gray boxes*. The chromosome (*Chr.*) number associated with each gene is provided. *Numbers at internodes* indicate supporting bootstrap values after 1000 iterations. Branch lengths represent the relative amount of molecular divergence as indicated in the *scale bar* (standardized rate of amino acid replacements per site). *B*, synteny analysis of human and zebrafish *Kcnh1* loci reveal conservation of gene clusters in fish and man. *C*, shown is exon distribution and amino acid identities among Kcnh1 proteins. Exon lengths in base pairs are indicated for human (*KCNH1*) and zebrafish (*kcnh1a/b*) genes. Conserved structural domains of the Kcnh1 proteins are assigned to the corresponding coding exons, and the identity of amino acid sequences between all three proteins is indicated below. *D*, membrane topology and domain structure of a single Kcnh1 subunit is shown. The positively charged voltage-sensor helix and the two pore helices are indicated in *gray* and *black*, respectively. *PAS*, Per-ARNT-Sim domain; *cNBD*, cyclic nucleotide-binding domain. Binding sites for Ca^{2+}/CaM are shown as *black ovals*.

non-stationary noise analysis applied to on-cell patch clamp recordings at various voltages (Fig. 2*D*). The single-channel conductance was estimated by linear data fits to the single-channel current as a function of voltage. Both zebrafish channels had a higher single-channel conductance than human KCNH1 (11.1 ± 0.5 picosiemens (pS); $n = 5$), with 13.5 ± 0.6 pS ($n = 4$) for Kcnh1a and 18.1 ± 0.9 pS ($n = 7$) for Kcnh1b. The extrapolated reversal potentials, between −45 and −50 mV in all cases, indicated a strong selectivity of all three channels for K^+ over Na^+ ions.

Hallmarks of mammalian Kcnh1 channels are two unique features; 1) extracellular Mg^{2+} ions markedly slow down activation (43, 44), and 2) intracellular Ca^{2+}/CaM inhibit current conduction (36). Two-electrode voltage clamp experiments shown in Fig. 3*A* demonstrate that 5 mM Mg^{2+} in the external solution slows the activation of all three channel types with similar potency. Normalized current values, reached after 20 ms, revealed a slightly stronger effect of external Mg^{2+} on both zebrafish channels compared with human KCNH1. The current ratios (I [Mg^{2+}]/I [noMg^{2+}]) at 20 ms were 0.09 ± 0.01 ($n = 5$) and 0.06 ± 0.02 ($n = 5$) for Kcnh1a and Kcnh1b, respectively, and 0.21 ± 0.07 ($n = 5$) for human KCNH1.

Channel regulation by Ca^{2+}/CaM was analyzed using single-step depolarizations of inside-out membrane patches to 40 mV. Fig. 3*B* shows current traces from representative experiments before and after application of 1 μM Ca^{2+} and 100 nM CaM to the cytosolic membrane face. Analysis of the remaining currents after Ca^{2+}/CaM application did not show significant differences between KCNH1 and the zebrafish channels. In summary, cloning and expression of two *kcnh1* genes from zebrafish revealed that both genes encode functional voltage-gated potassium channels, sharing the characteristic biophysical features of human KCNH1 channels.

Given the functional and structural similarities between both zebrafish channel paralogs, we wondered if Kcnh1a and Kcnh1b are able to form heteromeric channels. After a previously described experimental approach (25, 45), we generated dominant negative mutants of both channels by single amino acid replacements (G438C) in the selectivity filter. mRNA encoding the mutant zebrafish channels as well as a dominant negative human *KCNH1* variant (25) were each co-injected with wild-type mRNA for the zebrafish channels (Fig. 3*C*). All three mutant constructs led to reduced current amplitudes of Kcnh1a and Kcnh1b channels, strongly suggesting that both zebrafish paralogs can form hetero-tetrameric channels with each other as well as with the human KCNH1 channel. A nonspecific current reduction via an excess of mRNA could be excluded, as comparable high amounts of the respective wild-type mRNAs resulted in increased current amplitudes (not shown).

Both Zebrafish kcnh1 Genes Are Expressed in Neural Tissue—We analyzed the temporal gene expression patterns of *kcnh1a* and *kcnh1b* by RT-PCR at different developmental stages. Both paralogs were expressed maternally and could be detected in all developmental stages analyzed (Fig. 4*A*). The expression levels of both genes were stable until 11 hpf and increased significantly thereafter, displaying constantly high levels until 5 days post-fertilization. Interestingly, the time point around 14 hpf marks the start of neurulation in zebrafish.

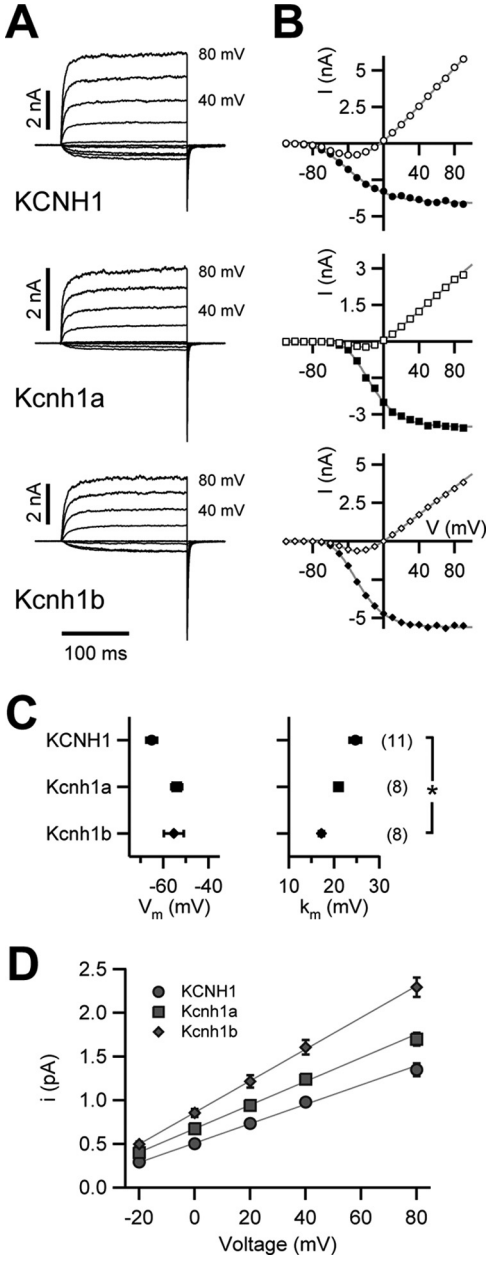

FIGURE 2. **Electrophysiological properties of Kcnh1 channels expressed in *Xenopus* oocytes.** *A*, current-voltage relationships were determined in inside-out patch configuration. Shown are superimposed current traces for depolarizing 200-ms steps ranging from −110 to +100 mV (from a holding potential of −120 mV) in steps of 10 mV at an interval of 5 s (only traces between −100 and +80 mV are shown, step size 20 mV; +80- and +40-mV traces are labeled). *B*, shown is mean current within the last 50 ms of the depolarizing steps (*open symbols*) and peak tail currents at −120 mV (*filled symbols*) as a function of the test voltage. Superimposed *gray curves* are fits according to a 4th-order Boltzmann function (tail currents) or a 4th-order Boltzmann function with consideration of a linear conductance (mean currents), yielding a half-maximal voltage of gate activation (V_m) and a corresponding slope factor (k_m). *C*, shown are the results of the analysis of steady-state voltage dependence of activation; V_m and k_m as the mean ± S.E. The numbers of experiments for *A–C* are shown in *parentheses*; * denotes statistical difference to the value obtained for KCNH1 with $p < 0.05$ (Student's *t* test). *D*, single-channel conductance determination for zebrafish Kcnh1 channels and human KCNH1 are shown. Single-channel current amplitudes are plotted as a function of test voltage determined with non-stationary noise analysis from on-cell membrane patches. *Error bars* denote S.E. values ($n = 4–7$). The *straight lines* are linear fits to estimate the single-channel conductance.

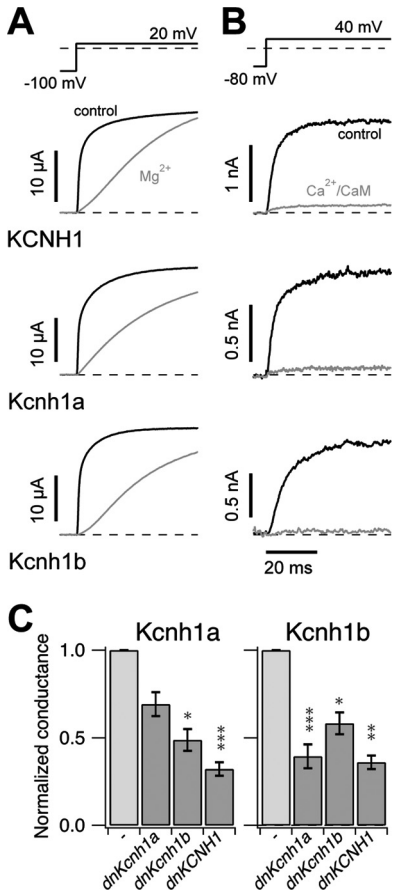

FIGURE 3. **Kcnh1-specific characteristics of channel activation and inhibition.** *A*, shown is dependence of channel activation on prepulse potential and Mg^{2+} ions. Current traces elicited by depolarizing 300-ms steps to 20 mV from holding potentials as indicated in the corresponding pulse protocol (*upper panel*) were measured in the absence (*black curves*) and presence (*gray curves*) of external 5 mM Mg^{2+} ions. Measurements were performed using two-electrode voltage clamp. *B*, channel inhibition by Ca^{2+}/CaM is shown. Superimposition of current traces before (*black*) and 100 s after (*gray*) internal application of 100 nM CaM + 1 µM Ca^{2+} was measured from inside-out oocyte patches. Normalized residual currents in Ca^{2+}/CaM were 12.6 ± 4.3, 18.9 ± 7.1, and 8.8 ± 5.7% for KCNH1 ($n = 4$), Kcnh1a ($n = 5$), and Kcnh1b ($n = 5$), respectively. *C*, Kcnh1 channels can form heteromers. mRNA encoding dominant-negative (*dn*) mutants of Kcnh1a (G438C), Kcnh1b (G438C), or human KCNH1 (G440C) were co-injected at 1:1 ratio with wild-type mRNA of *Kcnh1a* or *Kcnh1b*, respectively. Using two-electrode voltage clamp, K^+ currents were elicited by stepwise depolarization (as in Fig. 2*A*), and the maximal conductances (G_{max}) were determined. The *bars* show the mean ± S.E. from three independent experiments ($n = 7–15$). All values are normalized to G_{max} measured after injection of wild-type channel mRNA alone. Student's *t* tests are indicated as * (<0.05), ** (<0.01), and *** (<0.001).

Analysis of the spatial distribution of mRNA levels in organs of adult zebrafish revealed distinct, but overlapping expression patterns of both paralogs (Fig. 4*B*). For *kcnh1a*, expression was highest in testis and brain, moderate in the eye and the gastrointestinal tract, and low in the heart. Strong expression of *kcnh1b* was observed in testis, whereas lower levels were detected in brain and ovary. *Kcnh1b* was also expressed in the gills, the kidney, and the intestine.

To analyze the spatial expression patterns during development, we performed whole-mount *in situ* hybridization experiments in embryos of different developmental stages using sequences within the least conserved last exons of both genes as probes. At 19 hpf, both paralogs showed weak but specific staining patterns; transcripts were detected in discrete domains of

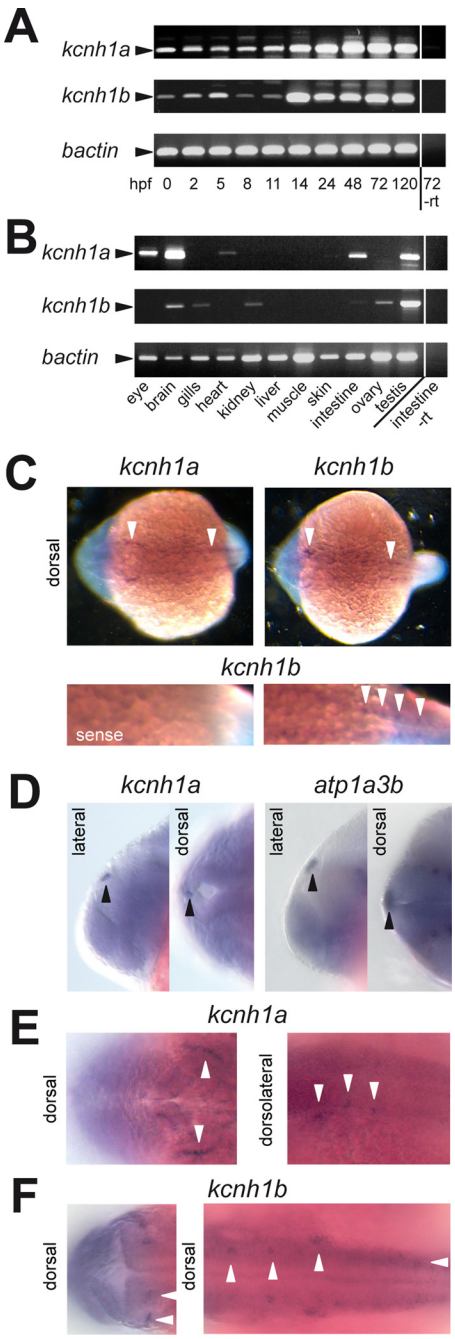

FIGURE 4. **Expression of *kcnh1a* and *kcnh1b* during early development and in the adult zebrafish.** *A*, temporal mRNA expression patterns of *kcnh1a* and *kcnh1b* in zebrafish embryos at the specified stages (in hours post fertilization, hpf) were analyzed by RT-PCR. One sample without reverse transcriptase (−*rt*) was used as a negative control. *bactin* was used as a housekeeping gene. *Arrowheads* indicate the expected amplicon sizes. *B*, shown is the expression pattern of *kcnh1a/b* in adult zebrafish tissues. mRNA was isolated from the specified organs, and analysis was performed as in *A*. *C–F*, dorsal and lateral views, anterior to the *left*, of zebrafish embryos at 19 hpf (*C*) and 24 hpf (*D–F*) were stained by whole-mount *in situ* hybridization. *Arrowheads* point to specific expression domains. *C*, *upper panels* show whole-mount staining for *kcnh1a* (*left*) and *kcnh1b* (*right*); the *lower panels* show enlarged posterior sections after *kcnh1b* staining (*right*) *versus* control staining with a *kcnh1b* sense probe (*left*). *D*, the *two left panels* (lateral and dorsal view) show an expression domain for *kcnh1a* (*arrowheads*) that was absent in *kcnh1b* staining. For comparison, the *right-hand images* show equivalent staining with an *atp1a3b*-specific probe that was previously shown to mark the epiphysis (30). *E*, image details show *kcnh1a* expression domains (*arrowheads*) in anterior (*left*, dorsal) and central to posterior parts (*right*, dorsolateral) of the embryo. *F*, dorsal view images in two focal planes show *kcnh1b* expression domains (*arrowheads*) in anterior (*left*) and central to posterior regions (*right*) of the embryo.

the hindbrain and trunk (Fig. 4*C*). Hindbrain expression was detectable in the rostrolateral part, anterior of the otic placode, most likely reflecting trigeminal ganglia (Fig. 4*C*, *upper panels*, *left arrowheads*). Expression of both paralogs in the trunk was confined to discrete spots arranged in bilateral rows (*top*, *right arrowheads* and *bottom*, *right panel*). This staining pattern likely reflects primary neurons such as Rohon-Beard neurons or motor neurons.

At the 24-hpf stage, a domain was detected in the dorsal midline of the brain expressing specifically *kcnh1a* (Fig. 4*D*, *left*), but not *kcnh1b* (not shown). This *kcnh1a*-specific domain closely resembled a staining of the epiphysis using the marker *atp1a3b* (30) as shown in Fig. 4*D*, *right*, for comparison.

As already seen at 19 hpf, *kcnh1a* expression domains at 24 hpf comprised a distinct, curved area in the hindbrain (Fig. 4*E*, *left*). In addition, three areas dorsal of the otic vesicle showed positive signals (Fig. 4*E*, *right*). In contrast, *kcnh1b* expression at 24 hpf was observed bilateral at two confined areas in the cerebellum (Fig. 4*F*, *left panel*) and in three prominently stained bilateral domains, two of which were located dorsomedial and another caudolateral from the otic vesicle (Fig. 4*F*, *right panel*, *upright arrowheads*). The dorsolateral *kcnh1b* expression domains along the trunk were less pronounced but still evident (Fig. 4*F*, *right panel*, *right arrowhead*). In summary, the expression patterns for *kcnh1a* and *kcnh1b* were overlapping but not identical.

Knockdown of kcnh1a or kcnh1b Induces Severe Developmental Disturbances—The maternal expression of *kcnh1a* and *kcnh1b* suggested a physiological function during early development (46). Because formation of neuronal structures is one of the earliest developmental processes, we hypothesized that neuronal expression of *kcnh1* genes might be of general importance for the growing embryo. To test this hypothesis we used a morpholino-mediated gene knockdown approach. MOs are antisense oligonucleotides that can prevent gene expression on two different levels (47). ATG morpholinos (ATG-MO) inhibit the translation of mature mRNAs. Alternatively, splice morpholinos (splice-MO) that are directed against specific splice donor or acceptor sites result in inclusion of an intron, exclusion of an exon, or usage of an alternative splice site. To rule out potential unspecific effects, we employed three different morpholinos for each *kcnh1* paralog, two splice-MO and one ATG-MO. In addition, one ATG-MO was designed to interfere with both paralogs (panATG-MO). As controls we used previously described ATG-MOs targeting the closely related *kcnh2* potassium channel gene or the *p53* tumor suppressor gene. Expression of *kcnh2* is confined to the heart, and knockdown of this gene has been reported to cause pericardial edemas, the absence of circulation, and atrioventricular block (13, 14). Knockdown of *p53* was reported to have no early phenotype, as expression of *p53* in zebrafish does not start before 48 hpf (32).

The most dramatic effect of all *kcnh1*-directed MO injections was a dose-dependent mortality of early embryos. Fig. 5*A* summarizes the survival rates at 24 h. Although uninjected controls and embryos injected with the *p53*-targeting morpholino had

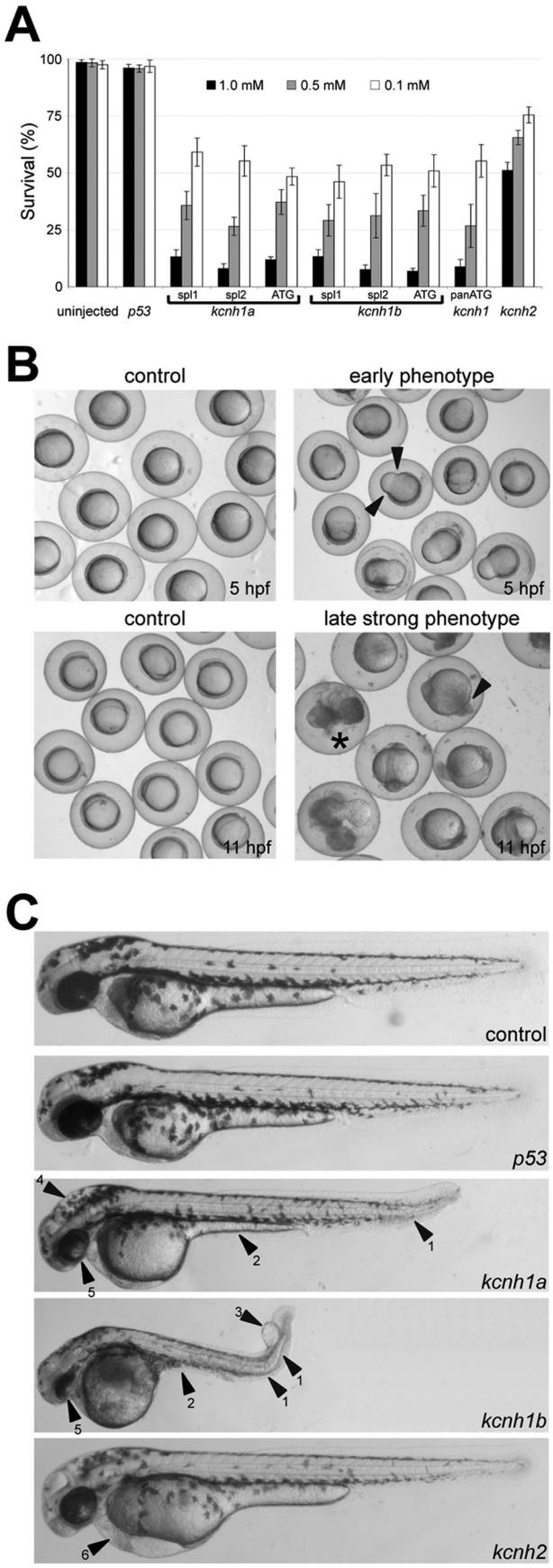

FIGURE 5. **Phenotype of *kcnh1a* and *kcnh1b* zebrafish morphants.** *A*, shown are survival rates of morphants at 24 h post-injection of the indicated MO concentrations. For both *kcnh1a* and *kcnh1b*, three different gene-specific MOs, affecting either splicing (spl1, spl2) or translation (ATG), were used to knock down gene function. A panATG MO was directed against both *kcnh1* paralogs. Uninjected embryos and embryos injected with MOs targeting *p53* or *kcnh2* genes served as controls. Results are based on four independent injections (mean ± S.E., $n = 20–50$). *B*, shown are two representative phenotypes of *kcnh1a* morphants after injection of ATG-interfering MOs (0.5 mM) at the indicated time points. *Arrowheads in the upper right image* indicate a typical constriction of the marginal enveloping cell layer at 5 hpf. At later stages (11 hpf), a strong phenotype was characterized by progressive cell detachment at the tail region (*lower right panel*, *arrowhead*), and subsequent necrosis (*asterisk*). *C*, shown is a phenotype of *kcnh1* morphants at 48 hpf in comparison to uninjected controls and *p53* or *kcnh2* morphants. All injections were performed with ATG-MO at 0.5 mM. Note the general growth retardation of *kcnh1* morphants and frequent characteristics, such as kinked tails (*arrowhead 1*), yolk-sac extension defects (*2*), tail edemas (*3*), hydrocephaly (*4*), and poorly developed eyes (*5*). The *bottom image* shows a *kcnh2* morphant with typical heart edema (*arrowhead 6*).

almost 100% survival rates, all morpholinos targeting *kcnh1* genes caused a dramatic reduction of survival irrespective of the mode of interference of the morpholino. At the lowest morpholino concentration (0.1 mM) about 50% of the morphants survived, and at the maximum concentration of 1 mM, the survival dropped below 20%. Apparently, both *kcnh1* paralogs must be involved in vital functions during development of the first 24 h. Knockdown of the *kcnh2* potassium channel gene had a milder phenotype and even at the highest concentration at least 50% of the embryos survived.

The earliest morphologic phenotype of *kcnh1* morphants was a constriction of the marginal enveloping cell layer (Fig. 5*B*, *upper right panel*). In seven independent injections with three different morpholinos for each of the two *kcnh1* paralogs as well as with the pan-ATG MO (all at 0.5 mM), this phenotype was detectable in 15- 30% of the injected embryos ($n \geq 75$) at 5 hpf. This constriction did not occur in any of the three controls. Later, at 11 hpf, 16–37% of the *kcnh1* morphants showed a strong phenotype with progressive cell detachment at the tails and eventually necrosis (Fig. 5*B*, *lower right image*). At 18 hpf most embryos had not developed further, and only 7–21% of the injected embryos in the seven groups of *kcnh1* morphants showed no severe malformations but were clearly retarded in growth compared with uninjected embryos. Given the severity of the phenotype in early development, we assume that these embryos are hypomorphic, most likely due to incomplete *kcnh1* knockdown.

Inspection of surviving morphants at 48 hpf revealed an overall growth retardation in all *kcnh1* morphants, irrespective of morpholino type (Fig. 5*C*). Beyond this general phenotype, frequently observed characteristics of *kcnh1* morphants were kinked tails (Fig. 5*C*, *arrowhead 1*), yolk sac extension defects (2), tail edemas (3), hydrocephaly (4), and poorly developed eyes (5). By contrast, *p53* morphants showed no differences in comparison to uninjected controls. The *kcnh2* morphants showed no growth retardation, but more than 50% of these embryos displayed typical heart edema (Fig. 5*C*, *bottom*, *arrowhead 6*).

To confirm efficiency and specificity of the morpholinos targeting *kcnh1a* and *kcnh1b*, we employed two strategies. First, we compared the efficiency of ATG-MOs on the protein level using modified GFP and RFP constructs harboring the morpholino target sequences upstream of the respective start codon supplemental Fig. S1, *A–C*; Table 1). Second, we exam-

ined the specificity and efficiency of *kcnh1* splice-MOs in knocking down the respective wild-type mRNAs using RT-PCR (supplemental Fig. S1*D*). The *kcnh1* ATG-MOs specifically blocked their target sequences supplemental Fig. S1C and Table 1), and the *kcnh1*splice-MOs specifically knocked down the levels of their target mRNAs in a dose-dependent manner supplemental Fig. S1*D*). The RT-PCR analyses also indicated lack of transcriptional compensation between *kcnh1* paralogs, as the knockdown of one *kcnh1* gene did not affect the mRNA levels of the other.

Knockdown of kcnh1a and kcnh1b Delays Hindbrain Formation and Somitogenesis—To gain insight into the events underlying the developmental defects in *kcnh1* morphants, we analyzed the expression pattern of developmental markers via whole-mount *in situ* hybridization in morphants with a mild phenotype. Analysis of early fate specification during gastrulation (5 hpf) using the axial mesoderm marker *no tail* (*ntl*) did not reveal any differences between *kcnh1a* and *kcnh1b* morphants and uninjected controls supplemental Fig. S2). However, during embryonic segmentation (12 hpf), *kcnh1a* and *kcnh1b* morphants consistently displayed a lateral expansion of hindbrain territories labeled by *krox20* (rhombomeres 3 and 5, Fig. 6, *white arrowheads*). In *kcnh1* morphants, the rhombomeres 3 and 5 were thinner and wider than in controls, and rhombomere boundaries were less sharp. In *kcnh1b* morphants, often no *krox20*-positive cells had reached the midline axis of rhombomere 5 at this time point (Fig. 6, *white arrowheads* in the *upper dorsal panel*). Together these findings suggest that hindbrain development in *kcnh1* morphants is delayed by several hours.

Labeling of somites in the axial mesoderm with a *myoD* probe was also indicative of a slower development of *kcnh1* morphants. At 12 hpf the number of clearly distinguishable somites was reduced, and they failed to expand laterally as in the controls (Fig. 6, *black arrowheads* in the *lower dorsal panel*). These results indicate that *kcnh1* MO disturbed the normal extension of the embryonic anterioposterior axis (*myoD*) and affected hindbrain patterning as visualized by the neural fate marker *krox20*.

TABLE 1

Specific effects of ATG morpholinos on the translation of modified GFP and RFP mRNAs

Numbers of embryos show detectable GFP and RFP signal (GFP/RFP) at 24 hpf, after the co-injection of the indicated morpholinos and mRNAs.

Morpholino-target sequence mRNA	None	*kcnh1a*	*kcnh1b*	*kcnh1* pan
GFP/RFP	13/13	15/15	12/12	12/12
kcnh1a MO wt-GFP[a]/*kcnh1a* MO mm-RFP[b]	12/12	4/17	16/16	18/18
kcnh1b MO wt-GFP/*kcnh1b* MO mm-RFP	14/14	18/18	2/16	13/13
kcnh1 pan-MO wt-GFP/*kcnh1* pan-MO mm-RFP	12/12	16/16	20/20	3/15

[a] wt indicates that the morpholino target sequence has the wild-type sequence as indicated in supplemental Fig. S1, *A* and *B*.

[b] mm indicates that the morpholino target sequence has five mismatches as shown in supplemental Fig. S1*B*.

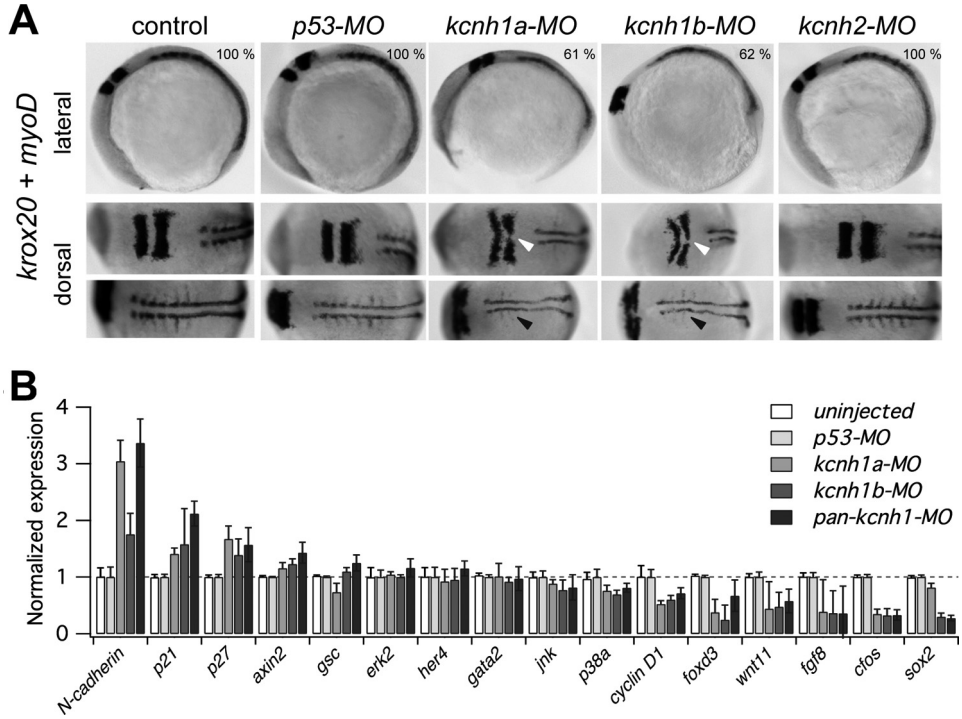

FIGURE 6. **Developmental delay of *kcnh1* morphants affects hindbrain formation and somitogenesis.** *A*, shown are representative whole-mount *in situ* hybridizations of zebrafish embryos with digoxigenin-labeled riboprobes for markers of hindbrain (*krox20*) and somites (*myoD*). Uninjected embryos (*control*) are compared with the indicated morphants. In lateral images (*upper row*), the dark-stained hindbrain rhombomeres 3 and 5 (*krox20*) and an extended stretch of *myoD*-stained somites are visible in the *upper left* and *right region of the images*, respectively. In the *bottom row* of the dorsal images the embryos are rotated to the left (anterior) by about 70 degrees. Note that in *kcnh1a* and *kcnh1b* morphants the rhombomeres 3 and 5 (*white arrows*) are thinner and that midline fusion of rhombomere 5 is incomplete. The lateral expansion and segmentation of somitic and presomitic mesoderm (*black arrows*) is reduced in both *kcnh1* morphants. The percentage of embryos showing the given phenotype in two independent experiments is indicated in the *upper images*. *B*, early gene expression is modulated by *kcnh1*. Expression of the indicated genes in zebrafish morphants was analyzed by quantitative RT-PCR at 70% epiboly stage (7.5 hpf). Gene-specific quantitative PCR signals in uninjected controls as well as in *kcnh1a*, *kcnh1b*, and pan-*kcnh1* morphants were normalized to *p53*-MO-injected controls, and *ef1a* served as the housekeeping gene for all samples. Genes are ordered according to the effect of *pan-kcnh1-MO* injection. Data are the mean ± S.D. from two independent experiments with each three reactions.

Knockdown of kcnh1 Alters the Expression of Genes Involved in Cell-cycle Control—To gain an insight into potential mechanisms underlying the described phenotype in *kcnh1* morphants, we used quantitative PCR and monitored the mRNA expression of genes required for zebrafish development. This gene set comprises transcription factors, cell-cycle regulators, protein kinases, and adhesion proteins. We assumed that the delay in hindbrain formation and somitogenesis at 12 hpf must be preceded by more subtle changes at earlier time points and chose the onset of constriction of the enveloping layer (70% epiboly, 7.5 hpf) for expression analysis. Consistent with our viability data (Fig. 5*A*), the knockdown of *p53* had no significant impact compared with uninjected controls. Fig. 6*B* shows the changes of mRNA levels, ordered from up-regulated to down-regulated genes. At this time point, the mRNA levels of several genes showed no or only minor changes upon *kcnh1*-MO injection. Among the non-responsive genes are the protein kinase genes *erk2*, *her4*, *jnk*, and the transcription factor *gata2*. This demonstrates that gene expression in *kcnh1* morphants is not generally disturbed. By contrast, the expression of three genes (*N-cadherin*, *p21*, *p27*) was up-regulated by more than 50% in at least one of the morphant groups. The products of *p21* and *p27* are known for their function as cyclin-dependent kinase inhibitors and, thus, inhibitors of cell proliferation. Also N-cadherin (*cdh2*) has recently been shown to restrict cell proliferation in zebrafish embryos (48). The up-regulation of N-cadherin was more pronounced in *kcnh1a* morphants and in embryos injected with the pan-*kcnh1*-MO than in *kcnh1b* morphants. A third group of genes was found down-regulated in *kcnh1* morphants. The respective gene products have diverse functions, including secreted signaling proteins (*wnt11*, *fgf8*), transcription factors (*foxD3*, *cfos*, *sox2*), and cell-cycle regulators (*cyclin D1*). Of note, the down-regulation of *cyclinD1* is in agreement with previous cell-based studies, reporting that siRNA targeting *kcnh1* down-regulates *cyclinD1* in human breast cancer cells (49). All the down-regulated genes are in one way or another associated with proliferation. Morpholino-induced gene repression was largely independent of the targeted *kcnh1* paralog, with exception of *sox2*, which was not significantly altered in *kcnh1a* morphants, but was strongly reduced by *kcnh1b*-MO and pan-*kcnh1*-MO (Fig. 6*B*). Taken together, the quantitative PCR data reveal that delayed patterning and growth reduction seen at 12 hpf in *knch1*-depleted zebrafish embryos are preceded by specific alterations in the transcription levels of genes involved in the control of cell proliferation. We were interested to see whether the impact of *kcnh1* knockdown on regulatory genes is predominantly quantitative or if the spatial expression of responsive genes is also disturbed. To address this question we selected three down-regulated genes (*fgf8*, *wnt11*, *foxd3*) and analyzed their expression domains by *in situ* hybridization at the gastrulation stage (90% epiboly) and during early somitogenesis supplemental Fig. S3). We did not observe prominent changes of the spatial expression profiles. However, a moderate reduction of signal intensity upon pan-*kcnh1*-MO injection was typically observed for *fgf8* and *foxd3* during gastrulation supplemental Fig. S3*A*).

DISCUSSION

The physiological and pathophysiological roles of the voltage-gated potassium channel Kcnh1 in humans and other mammals are far from being understood. Further investigations require suitable model organisms, allowing a faithful comparison to the situation in humans. We used zebrafish as a model to study expression and function of *kcnh1* genes during vertebrate embryogenesis. We found that fish *kcnh1* genes are duplicated (so called *kcnh1a* and *kcnh1b*) and highly conserved compared with the human ortholog. In adult fish we observed expression of both genes in the brain and expression of *kcnh1a* in the eye, which is consistent with the expression patterns found in mammals (3, 5). *Kcnh1* inactivation led to severe and lethal phenotypes. Molecular analysis of *kcnh1* loss-of-function phenotypes revealed a general delay of development in *kcnh1* morphants. The normal anterio-posterior patterning of zebrafish embryos is impaired, with evident loss of neural fate markers in the hindbrain region and reduced expression of muscle fate markers during segmentation. Our results thus suggest a crucial role of Kcnh1 channels during embryogenesis.

Electrophysiological characterization of heterologously expressed Kcnh1a and Kcnh1b channels revealed a functional behavior similar to that of the human channel but with slightly increased single-channel conductance of the fish channels. The typical modulation of channel activation kinetics by prepulse potential and external Mg^{2+} ions is also conserved between human and fish channels. This may be explained by almost complete conservation of the transmembrane segments S2 through S4, harboring the binding site for external Mg^{2+} ions (50). Similarly, the CaM binding motifs identified in the human KCNH1 channel (36, 51) are well conserved in the fish orthologs, and Ca^{2+} sensitivity of both fish channels could be confirmed in *Xenopus* oocytes.

After a whole-genome duplication event, a common fate of duplicated genes is the loss of function of one gene copy by inactivating mutations (52). Alternatively, preservation of two functional gene copies may occur if one gene adapts a new function (neofunctionalization) or if both genes experience a partial loss of subfunctions (53). In the case of the *kcnh1* genes in zebrafish, our heterologous expression data do not support neofunctionalization or loss of subfunctions. The analysis of mRNA expression of *kcnh1a* and *kcnh1b* in the developing embryo did not reveal evidence for temporal subfunctionalization, and both mRNA species were already present in the fertilized egg. We hypothesize that the two *kcnh1* paralogs underwent at least in part a spatial subfunction partitioning, as we observed overlapping but not identical expression domains for the two genes. This is exemplified by the exclusive detection of mRNA for *kcnh1a* in the epiphysis at 24 hpf, whereas at the same developmental stage three bilateral domains exhibited prominent and exclusive staining for *kcnh1b*. For domains that coexpress both paralogs (*e.g.* primary neurons along the body axis), the formation of heteromeric channels must be assumed, as simultaneous expression in *Xenopus* oocytes provided evidence for mixed channel formation. This is in agreement with the previous observation that human channels of the EAG subfamily (KCNH1, KCNH5) also form heteromers (25). Func-

tional coassembly of closely related channels has also been described for human eag-related gene (ERG) channels (45).

To date, the developmental activity of *kcnh1* genes has not been reported in mammalian models nor have embryonic phenotypes been described in *Drosophila eag* mutants. Early development is regulated by a combination of maternal factors (deposited in the egg during embryogenesis) and zygotic factors generated by the embryo itself (46). Our data indicate that zebrafish *kcnh1a* and *kcnh1b* are two of such maternal factors crucial for development. The knockdown of either one of the *kcnh1* genes led to severe phenotypes including early mortality and cell detachment.

In line with the predominantly neuronal expression of both *kcnh1* genes, an obvious late effect of morpholino treatment was an initial retardation of the developing brain accompanied by the loss of hindbrain markers. With ongoing development, these effects extended to other parts of the body including the tail, and the whole embryos did not reach normal length. In this context it is important to note that expression of both *kcnh1* paralogs was not restricted to the brain but was also detectable along the body axis in primary neurons of the spinal cord. Thus, the observed fundamental role of both *kcnh1* paralogs is in line with the temporal and spatial expression patterns of both genes.

Morpholino antisense technology provides a powerful tool to study gene function *in vivo*, but off-target effects have also been described to cause neural cell death and even general retardation (54). To exclude misinterpretations, we controlled our MO experiments in two ways, 1) by comparing our *kcnh1* morphant phenotypes with two independent MO and 2) by analyzing the extent of interference with normal *kcnh1* pre mRNA splicing via RT-PCR and expression of modified GFP/RFP mRNAs.

Although the morpholino-induced phenotypic alterations became apparent with the development of early brain structures and the onset of segmentation, changes in the transcriptional profile of distinct genes were already evident at 7.5 hpf (70% epiboly). Some of the observed changes like the up-regulation of cell-cycle inhibitors *p21* and *p27* immediately suggest a mechanistic basis for the developmental delay at later time points. For the cell adhesion protein N-cadherin (*cdh2*), a causal link of up-regulation to the phenotypic changes is less intuitive, but a specific role for N-cadherin in zebrafish neural development has recently been demonstrated (48). N-cadherin was found to restrict cell proliferation in the dorsal neural tube, a mechanism that might well be involved in the impaired neural development of *kcnh1* morphants. Principally, the impact of *kcnh1* knockdown on responsive genes might also involve a spatial disorganization of expression, in addition to quantitative effects. However, our analysis of *fgf8*, *wnt11*, and *foxd3* at later developmental stages did not reveal prominent changes in the respective expression patterns.

It remains to be determined how Kcnh1 proteins can influence gene expression in the developing embryo. The unique dependence of Kcnh1 channels on intracellular Ca^{2+}, distinguishing it from Kcnh2 and other voltage-gated potassium channels, may be of special interest because Ca^{2+}-dependent signals have a fundamental role in cellular signaling and a role for Ca^{2+} in patterning of the early zebrafish embryo is well established (for review, see Webb and Miller (55)). A recent report showing that human and rat Kcnh1 channels can also localize to the inner nuclear membrane (56) suggests that direct interactions with nuclear regulators and even with chromatin might also occur. Interestingly, of nine genes that we found regulated by *kcnh1* depletion, two genes were affected specifically by *kcnh1a* (*N-cadherin*) or by *kcnh1b* (*sox2*), suggesting that some regulatory functions of the paralogs must be unique. Given that critical players in embryogenesis are often re-employed in tumorigenesis, the disclosed role of Kcnh1 in ontogenetic processes will also have consequences for the future understanding of Kcnh1 channels in cell proliferation and cancer.

Acknowledgments—We thank Wolfgang Driever for help in interpreting expression patterns, Birgit Perner for sharing expertise in microscopy and Angela Roβner, Steffi Arend as well as Christin Hahn for excellent technical support. We thank Ulrike Gausmann for valuable help with bioinformatic analysis.

REFERENCES

1. Kaplan, W. D., and Trout, W. E. (1969) The behavior of four neurological mutants of *Drosophila*. *Genetics* **61,** 399–409
2. Ganetzky, B., and Wu, C. F. (1983) Neurogenetic analysis of potassium currents in *Drosophila*. Synergistic effects on neuromuscular transmission in double mutants. *J. Neurogenet.* **1,** 17–28
3. Ludwig, J., Weseloh, R., Karschin, C., Liu, Q., Netzer, R., Engeland, B., Stansfeld, C., and Pongs, O. (2000) Cloning and functional expression of rat eag2, a new member of the ether-à-go-go family of potassium channels and comparison of its distribution with that of eag1. *Mol. Cell. Neurosci.* **16,** 59–70
4. Martin, S., Lino de Oliveira, C., Mello de Queiroz, F., Pardo, L. A., Stühmer, W., and Del Bel, E. (2008) Eag1 potassium channel immunohistochemistry in the CNS of adult rat and selected regions of human brain. *Neuroscience* **155,** 833–844
5. Saganich, M. J., Machado, E., and Rudy, B. (2001) Differential expression of genes encoding subthreshold-operating voltage-gated K^+ channels in brain. *J. Neurosci.* **21,** 4609–4624
6. Bijlenga, P., Occhiodoro, T., Liu, J. H., Bader, C. R., Bernheim, L., and Fischer-Lougheed, J. (1998) An ether -à-go-go K^+ current, Ih-eag, contributes to the hyperpolarization of human fusion-competent myoblasts. *J. Physiol.* **512,** 317–323
7. Occhiodoro, T., Bernheim, L., Liu, J. H., Bijlenga, P., Sinnreich, M., Bader, C. R., and Fischer-Lougheed, J. (1998) Cloning of a human ether-a-go-go potassium channel expressed in myoblasts at the onset of fusion. *FEBS Lett.* **434,** 177–182
8. Pardo, L. A., del Camino, D., Sánchez, A., Alves, F., Brüggemann, A., Beckh, S., and Stühmer, W. (1999) Oncogenic potential of EAG K^+ channels. *EMBO J.* **18,** 5540–5547
9. Gavrilova-Ruch, O., Schönherr, K., Gessner, G., Schönherr, R., Klapperstück, T., Wohlrab, W., and Heinemann, S. H. (2002) Effects of imipramine on ion channels and proliferation of IGR1 melanoma cells. *J. Membr. Biol.* **188,** 137–149
10. Hemmerlein, B., Weseloh, R. M., Mello de Queiroz, F., Knötgen, H., Sánchez, A., Rubio, M. E., Martin, S., Schliephacke, T., Jenke, M., Heinz-Joachim-Radzun, Stühmer, W., and Pardo, L. A. (2006) Overexpression of Eag1 potassium channels in clinical tumors. *Mol. Cancer* **5,** 41
11. Spitzner, M., Ousingsawat, J., Scheidt, K., Kunzelmann, K., and Schreiber, R. (2007) Voltage-gated K^+ channels support proliferation of colonic carcinoma cells. *FASEB J.* **21,** 35–44
12. Kalluri, R., and Weinberg, R. A. (2009) The basics of epithelial-mesenchymal transition. *J. Clin. Invest.* **119,** 1420–1428
13. Arnaout, R., Ferrer, T., Huisken, J., Spitzer, K., Stainier, D. Y., Tristani-Firouzi, M., and Chi, N. C. (2007) Zebrafish model for human long QT syndrome. *Proc. Natl. Acad. Sci. U.S.A.* **104,** 11316–11321
14. Hassel, D., Scholz, E. P., Trano, N., Friedrich, O., Just, S., Meder, B., Weiss, D. L., Zitron, E., Marquart, S., Vogel, B., Karle, C. A., Seemann, G., Fish-

man, M. C., Katus, H. A., and Rottbauer, W. (2008) Deficient zebrafish ether-à-go-go-related gene channel gating causes short-QT syndrome in zebrafish reggae mutants. *Circulation* **117,** 866–875
15. Langheinrich, U., Vacun, G., and Wagner, T. (2003) Zebrafish embryos express an orthologue of HERG and are sensitive toward a range of QT-prolonging drugs inducing severe arrhythmia. *Toxicol. Appl. Pharmacol.* **193,** 370–382
16. Milan, D. J., Peterson, T. A., Ruskin, J. N., Peterson, R. T., and MacRae, C. A. (2003) Drugs that induce repolarization abnormalities cause bradycardia in zebrafish. *Circulation* **107,** 1355–1358
17. Mittelstadt, S. W., Hemenway, C. L., Craig, M. P., and Hove, J. R. (2008) Evaluation of zebrafish embryos as a model for assessing inhibition of hERG. *J. Pharmacol. Toxicol. Methods* **57,** 100–105
18. Scholz, E. P., Niemer, N., Hassel, D., Zitron, E., Bürgers, H. F., Bloehs, R., Seyler, C., Scherer, D., Thomas, D., Kathöfer, S., Katus, H. A., Rottbauer, W. A., and Karle, C. A. (2009) Biophysical properties of zebrafish ether-à-go-go-related gene potassium channels. *Biochem. Biophys. Res. Commun.* **381,** 159–164
19. Brugada, R., Hong, K., Dumaine, R., Cordeiro, J., Gaita, F., Borggrefe, M., Menendez, T. M., Brugada, J., Pollevick, G. D., Wolpert, C., Burashnikov, E., Matsuo, K., Wu, Y. S., Guerchicoff, A., Bianchi, F., Giustetto, C., Schimpf, R., Brugada, P., and Antzelevitch, C. (2004) Sudden death associated with short-QT syndrome linked to mutations in HERG. *Circulation* **109,** 30–35
20. Sanguinetti, M. C., Jiang, C., Curran, M. E., and Keating, M. T. (1995) A mechanistic link between an inherited and an acquired cardiac arrhythmia. HERG encodes the IKr potassium channel. *Cell* **81,** 299–307
21. Sanguinetti, M. C., and Tristani-Firouzi, M. (2006) hERG potassium channels and cardiac arrhythmia. *Nature* **440,** 463–469
22. Kimmel, C. B., Ballard, W. W., Kimmel, S. R., Ullmann, B., and Schilling, T. F. (1995) Stages of embryonic development of the zebrafish. *Dev. Dyn.* **203,** 253–310
23. Kumar, S., Tamura, K., and Nei, M. (1994) MEGA. Molecular evolutionary genetics analysis software for microcomputers. *Comput. Appl. Biosci.* **10,** 189–191
24. Liman, E. R., Tytgat, J., and Hess, P. (1992) Subunit stoichiometry of a mammalian K^+ channel determined by construction of multimeric cDNAs. *Neuron* **9,** 861–871
25. Schönherr, R., Gessner, G., Löber, K., and Heinemann, S. H. (2002) Functional distinction of human EAG1 and EAG2 potassium channels. *FEBS Lett.* **514,** 204–208
26. Hauptmann, G., and Gerster, T. (1994) Two-color whole-mount *in situ* hybridization to vertebrate and *Drosophila* embryos. *Trends Genet.* **10,** 266
27. Schulte-Merker, S., Ho, R. K., Herrmann, B. G., and Nüsslein-Volhard, C. (1992) The protein product of the zebrafish homologue of the mouse T gene is expressed in nuclei of the germ ring and the notochord of the early embryo. *Development* **116,** 1021–1032
28. Weinberg, E. S., Allende, M. L., Kelly, C. S., Abdelhamid, A., Murakami, T., Andermann, P., Doerre, O. G., Grunwald, D. J., and Riggleman, B. (1996) Developmental regulation of zebrafish MyoD in wild-type, no tail, and spadetail embryos. *Development* **122,** 271–280
29. Oxtoby, E., and Jowett, T. (1993) Cloning of the zebrafish krox-20 gene (krx-20) and its expression during hindbrain development. *Nucleic Acids Res.* **21,** 1087–1095
30. Thisse, B., Pflumio, S., Fürthauer, M., Loppin, B., Heyer, V., Degrave, A., Woehl, R., Lux, A., Steffan, T., Charbonnier, X., and Thisse, C. (2001) *ZFIN Direct Data Submission*, available online
31. Reifers, F., Böhli, H., Walsh, E. C., Crossley, P. H., Stainier, D. Y., and Brand, M. (1998) Fgf8 is mutated in zebrafish acerebellar (ace) mutants and is required for maintenance of midbrain-hindbrain boundary development and somitogenesis. *Development* **125,** 2381–2395
32. Robu, M. E., Larson, J. D., Nasevicius, A., Beiraghi, S., Brenner, C., Farber, S. A., and Ekker, S. C. (2007) p53 activation by knockdown technologies. *PLoS Genet* **3,** e78
33. McCurley, A. T., and Callard, G. V. (2010) Time course analysis of gene expression patterns in zebrafish eye during optic nerve regeneration. *J. Exp. Neurosci.* **2010,** 17–33
34. Livak, K. J., and Schmittgen, T. D. (2001) Analysis of relative gene expression data using real-time quantitative PCR and the $2^{-\Delta\Delta CT}$ method. *Methods* **25,** 402–408
35. Wang, M. H. (2004) A technical consideration concerning the removal of oocyte vitelline membranes for patch clamp recording. *Biochem. Biophys. Res. Commun.* **324,** 971–972
36. Schönherr, R., Löber, K., and Heinemann, S. H. (2000) Inhibition of human ether à go-go potassium channels by Ca^{2+}/calmodulin. *EMBO J.* **19,** 3263–3271
37. Heinemann, S. H., and Conti, F. (1992) Nonstationary noise analysis and application to patch clamp recordings. *Methods Enzymol.* **207,** 131–148
38. Starkus, J. G., Varga, Z., Schönherr, R., and Heinemann, S. H. (2003) Mechanisms of the inhibition of Shaker potassium channels by protons. *Pflügers Arch.* **447,** 44–54
39. Kohn, M., Högel, J., Vogel, W., Minich, P., Kehrer-Sawatzki, H., Graves, J. A., and Hameister, H. (2006) Reconstruction of a 450-My-old ancestral vertebrate protokaryotype. *Trends Genet* **22,** 203–210
40. Amores, A., Force, A., Yan, Y. L., Joly, L., Amemiya, C., Fritz, A., Ho, R. K., Langeland, J., Prince, V., Wang, Y. L., Westerfield, M., Ekker, M., and Postlethwait, J. H. (1998) Zebrafish hox clusters and vertebrate genome evolution. *Science* **282,** 1711–1714
41. Taylor, J. S., Braasch, I., Frickey, T., Meyer, A., and Van de Peer, Y. (2003) Genome duplication, a trait shared by 22000 species of ray-finned fish. *Genome Res* **13,** 382–390
42. Venkatesh, B. (2003) Evolution and diversity of fish genomes. *Curr. Opin. Genet. Dev.* **13,** 588–592
43. Ludwig, J., Terlau, H., Wunder, F., Brüggemann, A., Pardo, L. A., Marquardt, A., Stühmer, W., and Pongs, O. (1994) Functional expression of a rat homologue of the voltage gated either á go-go potassium channel reveals differences in selectivity and activation kinetics between the *Drosophila* channel and its mammalian counterpart. *EMBO J.* **13,** 4451–4458
44. Schönherr, R., Mannuzzu, L. M., Isacoff, E. Y., and Heinemann, S. H. (2002) Conformational switch between slow and fast gating modes. Allosteric regulation of voltage sensor mobility in the EAG K^+ channel. *Neuron* **35,** 935–949
45. Wimmers, S., Wulfsen, I., Bauer, C. K., and Schwarz, J. R. (2001) Erg1, erg2 and erg3 K^+ channel subunits are able to form heteromultimers. *Pflügers Arch.* **441,** 450–455
46. Pelegri, F. (2003) Maternal factors in zebrafish development. *Dev. Dyn.* **228,** 535–554
47. Summerton, J. (1999) Morpholino antisense oligomers. The case for an RNase H-independent structural type. *Biochim. Biophys. Acta* **1489,** 141–158
48. Chalasani, K., and Brewster, R. M. (2011) N-cadherin-mediated cell adhesion restricts cell proliferation in the dorsal neural tube. *Mol. Biol. Cell* **22,** 1505–1515
49. Borowiec, A. S., Hague, F., Gouilleux-Gruart, V., Lassoued, K., and Ouadid-Ahidouch, H. (2011) Regulation of IGF-1-dependent cyclin D1 and E expression by hEag1 channels in MCF-7 cells. The critical role of hEag1 channels in G_1 phase progression. *Biochim. Biophys. Acta* **1813,** 723–730
50. Silverman, W. R., Tang, C. Y., Mock, A. F., Huh, K. B., and Papazian, D. M. (2000) Mg^{2+} modulates voltage-dependent activation in ether-à-go-go potassium channels by binding between transmembrane segments S2 and S3. *J. Gen. Physiol.* **116,** 663–678
51. Ziechner, U., Schönherr, R., Born, A. K., Gavrilova-Ruch, O., Glaser, R. W., Malesevic, M., Küllertz, G., and Heinemann, S. H. (2006) Inhibition of human ether à go-go potassium channels by Ca^{2+}/calmodulin binding to the cytosolic N and C termini. *FEBS J.* **273,** 1074–1086
52. Ohno, S. (1970) *Evolution by Gene Duplication*, Springer-Verlag, Berlin, New York
53. Force, A., Lynch, M., Pickett, F. B., Amores, A., Yan, Y. L., and Postlethwait, J. (1999) Preservation of duplicate genes by complementary, degenerative mutations. *Genetics* **151,** 1531–1545
54. Heasman, J. (2002) Morpholino oligos. Making sense of antisense? *Dev. Biol.* **243,** 209–214
55. Webb, S. E., and Miller, A. L. (2007) Ca^{2+} signaling and early embryonic patterning during zebrafish development. *Clin. Exp. Pharmacol. Physiol.* **34,** 897–904
56. Chen, Y., Sánchez, A., Rubio, M. E., Kohl, T., Pardo, L. A., and Stühmer, W. (2011) Functional K(v)10.1 channels localize to the inner nuclear membrane. *PLoS One* **6,** e19257